

USAFSAM-TR-88-18

THEORETICAL MODELS FOR INTERACTION OF ELECTROMAGNETIC FIELDS WITH BIOLOGICAL TISSUES

Jeremy H. Nussbaum, Sc.D.
Alan J. Grodzinsky, Sc.D.

AD-A206 923

Laboratory for Electromagnetic and Electronic Systems
Massachusetts Institute of Technology
MIT, 38-377
Cambridge, MA 02139

January 1989

Final Report for Period July 1986 - July 1988

Approved for public release; distribution is unlimited.

Prepared for
USAF SCHOOL OF AEROSPACE MEDICINE
Human Systems Division (AFSC)
Brooks Air Force Base, TX 78235-5301



014

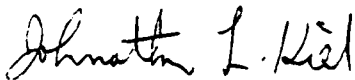
NOTICES

This final report was submitted by the Laboratory for Electromagnetic and Electronic Systems, Massachusetts Institute of Technology, MIT, 38-377, Cambridge, Massachusetts, under contract F33615-83-D-0601, job order 2312-W1-14, with the USAF School of Aerospace Medicine, Human Systems Division, AFSC, Brooks Air Force Base, Texas. Dr. Johnathan L. Kiel (USAFSAM/RZP) was the Laboratory Project Scientist-in-Charge.

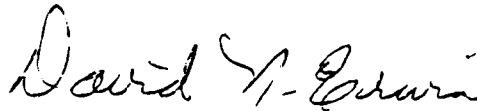
When Government drawings, specifications, or other data are used for any purpose other than in connection with a definitely Government-related procurement, the United States Government incurs no responsibility nor any obligation whatsoever. The fact that the Government may have formulated or in any way supplied the said drawings, specifications, or other data, is not to be regarded by implication, or otherwise in any manner construed, as licensing the holder or any other person or corporation; or as conveying any rights or permission to manufacture, use, or sell any patented invention that may in any way be related thereto.

The Office of Public Affairs has reviewed this report, and it is releasable to the National Technical Information Service, where it will be available to the general public, including foreign nationals.

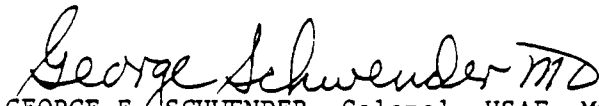
This report has been reviewed and is approved for publication.



JOHNATHAN L. KIEL, Ph.D.
Project Scientist



DAVID N. ERWIN, Ph.D.
Supervisor



GEORGE E. SCHWENDER, Colonel, USAF, MC, SFS
Commander

UNCLASSIFIED

SECURITY CLASSIFICATION OF THIS PAGE

REPORT DOCUMENTATION PAGE				Form Approved OMB No. 0704-0188	
1a. REPORT SECURITY CLASSIFICATION Unclassified			1b. RESTRICTIVE MARKINGS		
2a. SECURITY CLASSIFICATION AUTHORITY			3. DISTRIBUTION/AVAILABILITY OF REPORT Approved for public release; distribution is unlimited.		
2b. DECLASSIFICATION/DOWNGRADING SCHEDULE					
4. PERFORMING ORGANIZATION REPORT NUMBER(S)			5. MONITORING ORGANIZATION REPORT NUMBER(S) USAFSAM-TR-88-18		
6a. NAME OF PERFORMING ORGANIZATION Lab. for Electr & Electr Syst Massachusetts Inst. of Tech		6b. OFFICE SYMBOL (If applicable)	7a. NAME OF MONITORING ORGANIZATION USAF School of Aerospace Medicine (RZP)		
6c. ADDRESS (City, State, and ZIP Code) MIT, 38-377 Cambridge, MA 02139		7b. ADDRESS (City, State, and ZIP Code) Human Systems Division (AFSC) Brooks Air Force Base, TX 78235-5301			
8a. NAME OF FUNDING/SPONSORING ORGANIZATION		8b. OFFICE SYMBOL (If applicable)	9. PROCUREMENT INSTRUMENT IDENTIFICATION NUMBER F33615-83-D-0601		
8c. ADDRESS (City, State, and ZIP Code)		10. SOURCE OF FUNDING NUMBERS			
		PROGRAM ELEMENT NO. 61102F	PROJECT NO. 2312	TASK NO. W1	WORK UNIT ACCESSION NO. 14
11. TITLE (Include Security Classification) Theoretical Models for Interaction of Electromagnetic Fields with Biological Tissues					
12. PERSONAL AUTHOR(S) Nussbaum, Jeremy H.; Grodzinsky, Alan J.					
13a. TYPE OF REPORT Final		13b. TIME COVERED FROM 86/07/01 TO 88/07/01		14. DATE OF REPORT (Year, Month, Day) 1989, January	
15. PAGE COUNT 29					
16. SUPPLEMENTARY NOTATION					
17. COSATI CODES			18. SUBJECT TERMS (Continue on reverse if necessary and identify by block number)		
FIELD	GROUP	SUB-GROUP			
06	07		Models ; Electrodiffusion ;		
06	04		Membranes Biology ; Electromechanochemical effects ;		
19. ABSTRACT (Continue on reverse if necessary and identify by block number) This work demonstrates that electric fields can modulate intramembrane ionic concentrations, transmembrane ionic fluxes, mechanical conformation of membranes, and transmembrane potential. Even symmetrically applied fields of opposite polarities can result in asymmetric mechanical, concentration and flux responses, hence rectification of electrochemical and electromechanical phenomena can produce long-term effects even though the induced change is small. The general electromechanochemical model presented predicts rectification phenomena and includes mechanical and electromechanical conformational change dynamics. <i>Key words: radiofrequency radiation, electromagnetic radiation.</i>					
20. DISTRIBUTION/AVAILABILITY OF ABSTRACT <input checked="" type="checkbox"/> UNCLASSIFIED/UNLIMITED <input type="checkbox"/> SAME AS RPT <input type="checkbox"/> OTIC USERS			21. ABSTRACT SECURITY CLASSIFICATION Unclassified		
22a. NAME OF RESPONSIBLE INDIVIDUAL Johnathan L. Kiel			22b. TELEPHONE (Include Area Code) (512) 536-3583		22c. OFFICE SYMBOL USAFSAM/RZP

TABLE OF CONTENTS

	<u>page</u>
Introduction and Overview	1
Basic Electromechanical Transduction Mechanisms	3
Details of the Model	5
Case Study	11
Application of Theory to Biological Cases	16
Summary	20
Acknowledgments	23
References	23

Accession For	
NTIS GRA&I	<input checked="" type="checkbox"/>
DTIC TAB	<input type="checkbox"/>
Unannounced	<input type="checkbox"/>
Justification	
By _____	
Distribution/	
Availability Codes	
Dist	Avail and/or Special
A-1	



THEORETICAL MODELS FOR INTERACTION OF ELECTROMAGNETIC FIELDS WITH BIOLOGICAL TISSUES

INTRODUCTION AND OVERVIEW

Radiofrequency radiation can interact with biological tissues and membranes in many ways. In this study, a continuum approach to modelling transductive coupling in membranes and extracellular matrix was taken. The mechanism modelled was the mediation of transmembrane transport properties via electrodiffusion and electromechanical coupling.

Possible sites for such coupling include nerve cell and other cell membranes and their surrounding volumes, and larger membrane structures, such as extracellular matrix and epithelial membranes [1,2]. The effects on nerve cells and the surrounding regions could include changes in nerve impulse generation and transmission rates. In general, cell membrane permeability to selected solutes could be changed, leading to changes in metabolic and/or enzymatic rates and products, as well as changes in the intracellular ionic environment. Epithelial membrane permeability may be changed through changes in one or more of the basolateral and apical membrane, or the junctions.

The prototypical configuration shown in Figure 1 is used to gain insight into membrane response to applied electric fields. A membrane separates two baths of differing salt concentration and pH. The membrane matrix itself has charged sites attached to it, some of which may be ionized, and some of which are not. Here the fixed charge is represented by carboxylic acid groups. The membrane has a proportion of solid content and fluid content, which can change as the fixed charge and/or the local ionic environment changes. The proportion of liquid volume to solid volume is the hydration H . The membrane state is described by the fixed charge, hydration and ionic concentrations at each point, which in general will be functions of time.

We have constructed a theory, described originally in a doctoral thesis[3], which models in a self-consistent manner the coupling between an electric field applied

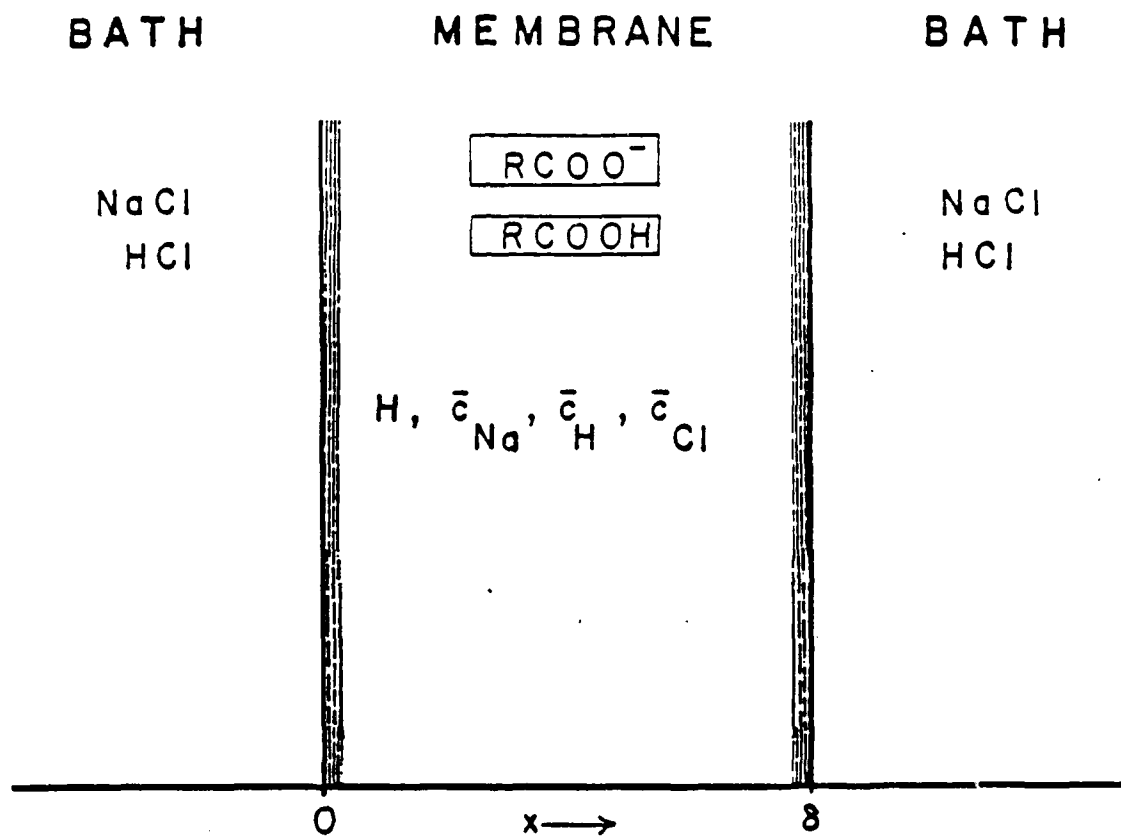


Figure 1. Case study of electromechanochemical transduction. A membrane with fixed charge density \bar{c}_m^* separates two baths with differing salt concentration c_{NaCl} and differing acid concentration c_{HCl} . The membrane ionic profiles \bar{c}_{H^+} , \bar{c}_{Na^+} and \bar{c}_{Cl^-} , the fixed charge density \bar{c}_m^* and hydration H are functions of time and space.

across the membrane configuration of Figure 1 and the intra-membrane ionic, fixed charge and concentration profiles, given the electromechanical and electrochemical properties of the membrane, and given the electrical mechanical and chemical boundary conditions imposed.

This model could be viewed as a black box, shown in Figure 2, into which the boundary conditions and membrane properties are input, and out of which we get the intramembrane ionic and hydration profiles, and quantities such as membrane thickness transmembrane voltage drop, ionic fluxes, and net current density. The black box can be included in a more comprehensive model of cellular response to an applied electric field, which might include, e.g., models of specific metabolic processes. Note that the type of electromechanical coupling could be modified to more accurately reflect what is actually occurring in the cell membrane.

BASIC ELECTROMECHANICAL TRANSDUCTION MECHANISMS

Changes in polyelectrolyte ionic environment have been shown to modify the electromechanochemical properties of the polyelectrolyte[4,5]. Two basic mechanisms of electromechanochemical transduction are considered. In each mechanism, the electrostatic repulsion force, or the free energy of a given configuration is modified by changes in the local ionic environment. In the fixed charge mechanism, the local fixed charge is modified by changes in local chemical environment, such as would happen when the local pH changes around a carboxylic acid residue. In the Debye length mechanism, the local excess salt concentration is changed, leading to changes in local electrostatic shielding (local Debye length).

The charge mechanism is illustrated in Figure 3. A cross-linked polyelectrolyte membrane is made up of many interconnected "strands" of linear polymer, with charged site on the polymer. In the absence of charge, a polymer strand will curl up, due to entropic forces. As the charge is increased, the electrostatic interactions increasingly favor an extended configuration. In the absence of mechanical constraints, a homogeneous isotropic polyelectrolyte membrane as a whole will expand when the fixed charge is increased. The charge may be changed due to chemical reaction, such as the charging of carboxylic acid sites.

The Debye length mechanism is illustrated in Figure 4. Here the number of fixed charges may remain the same, but the local ionic environment is changed. The electric field due to each charge decays over a characteristic length termed the Debye length. The shaded region in the figure schematically represents the Debye length. As the local ionic concentrations decrease, the Debye length increases, resulting in increased electrostatic interactions as the electric fields due to each charge increasingly overlap each other. In the absence of mechanical constraints, this results in a more swollen membrane.

MODEL: COUPLED ELECTRICAL, MECHANICAL, CHEMICAL INTERACTIONS IN IONIZABLE HYDROGELS

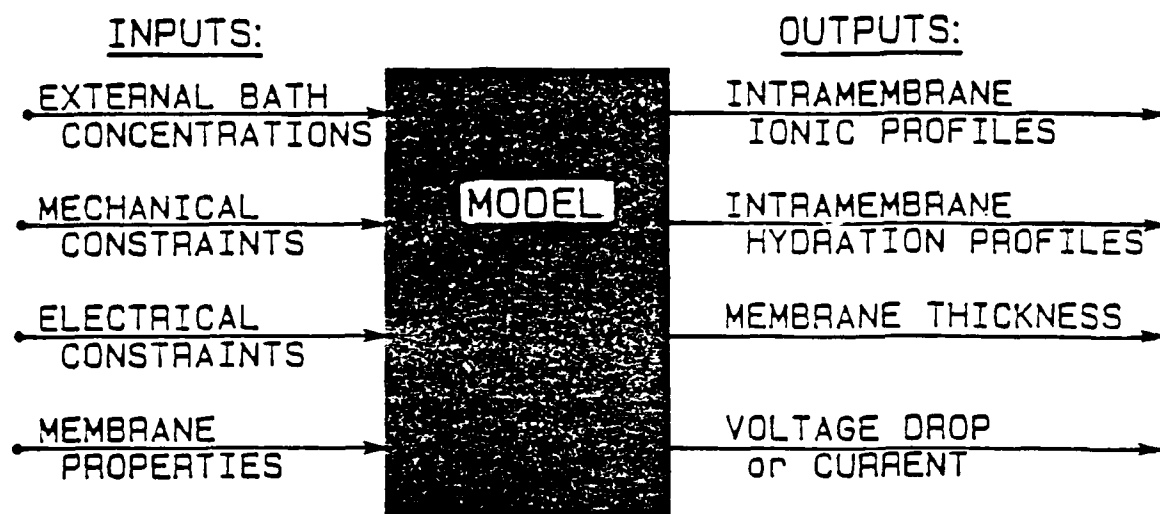


Figure 2. Black box representation of coupled electromechanochemical model of membrane transduction.

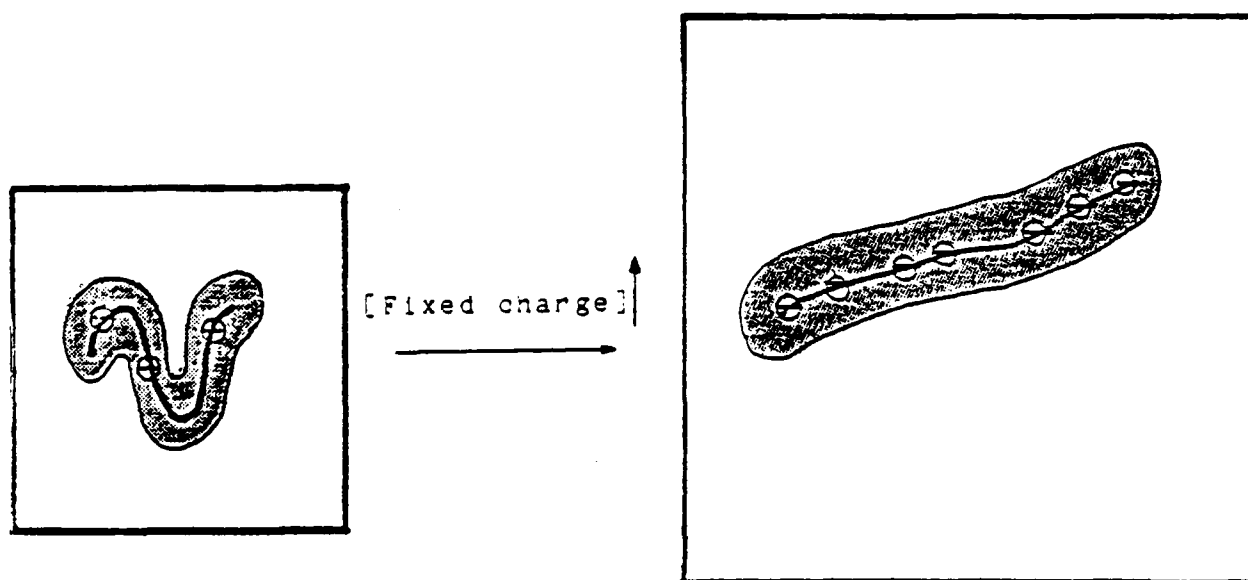


Figure 3. Charge mechanism of electromechanochemical transduction.

Basic electrodiffusion mechanisms are illustrated in Figure 5. A positively charged membrane separates two baths. The salt concentration is higher on the right than on the left. In the absence of an applied field, the co-ion concentration is approximately linear. The self-generated electric field due to unequal diffusivities of cation and anion affects the majority carrier, the counter ion almost exclusively. In the graph, normalized co-ion concentration is plotted vs. normalized position in the membrane. In the presence of an applied field, the steady state concentration profile bows, here in the direction of the applied field. As a stronger field is applied from left to right, the concentration in the bulk of the membrane is depleted. As the field is applied from right to left, the concentration in the bulk of the membrane is enhanced.

An applied field can thus change the intramembrane concentration profiles of hydrogen and salt ions, and in that fashion change the local swelling, through the charge effect and the Debye length effect. The phenomenon is shown in more detail in Figure 6. The four graphs show concentration and hydration profiles within a chargeable, swellable membrane separating two baths at different pH. The fixed charges are carboxylic acid groups with an estimated pK of 5.5. The bath at the left is at pH 3.5 and the bath at the right is at pH 6. The intramembrane pH at the boundary is not the same due to Donnan partitioning. At the upper right, we see the hydrogen ion profile at zero current is approximately linear. The membrane fixed charge profile, at the lower left, is fairly constant throughout the bulk of the membrane, with a sharp increase in fixed charge at the right-hand boundary, as the pH increases. The hydration too is fairly constant in the bulk, and increases rapidly at the right-hand side as the fixed charge increases rapidly. As a field is applied from right to left, the hydrogen ion profiles bow in that direction, resulting in significantly decreased hydrogen ion concentration in the bulk of the membrane. The decreased concentration, in turn, leads to an increase in the magnitude of membrane fixed charge, shown in the lower left. This increased magnitude, in turn, leads to an increase in hydration throughout the bulk of the membrane, shown in the lower right. The counter-ion concentration too increases in the bulk of the membrane as the magnitude of the fixed charge increases, as shown in the upper right. All of these profiles are based on the model presented in the next section.

DETAILS OF THE MODEL

The model attempts to account for the coupling between diffusion, migration and convection of ions, fluid transport and electromechanical and electrochemical coupling to the membrane in a self-consistent manner, including the effects of an applied electric field. It includes equations for all of these phenomena, and can be solved for the steady state profiles and for the transient response to an applied electric field.

Figure 7 shows the general form of the electrochemical equations. Ionic fluxes have a diffusive component, a migratory component and a convective component.

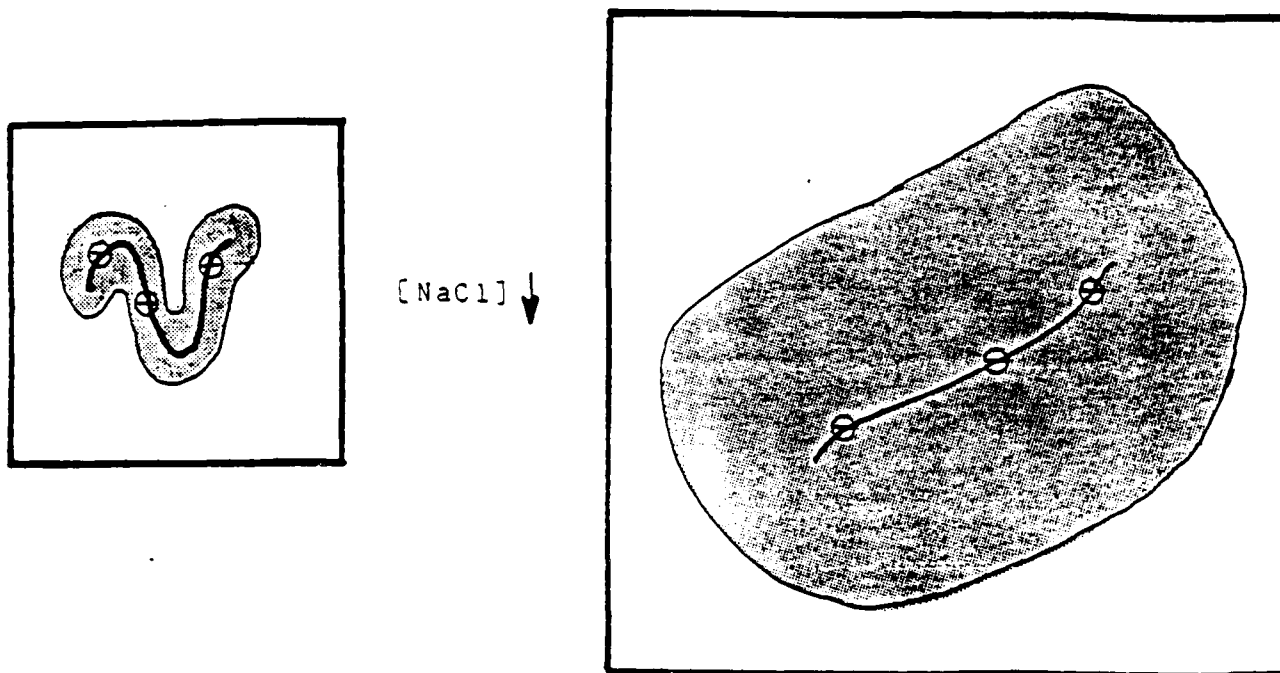


Figure 4. Debye length mechanism of electromechanochemical transduction.

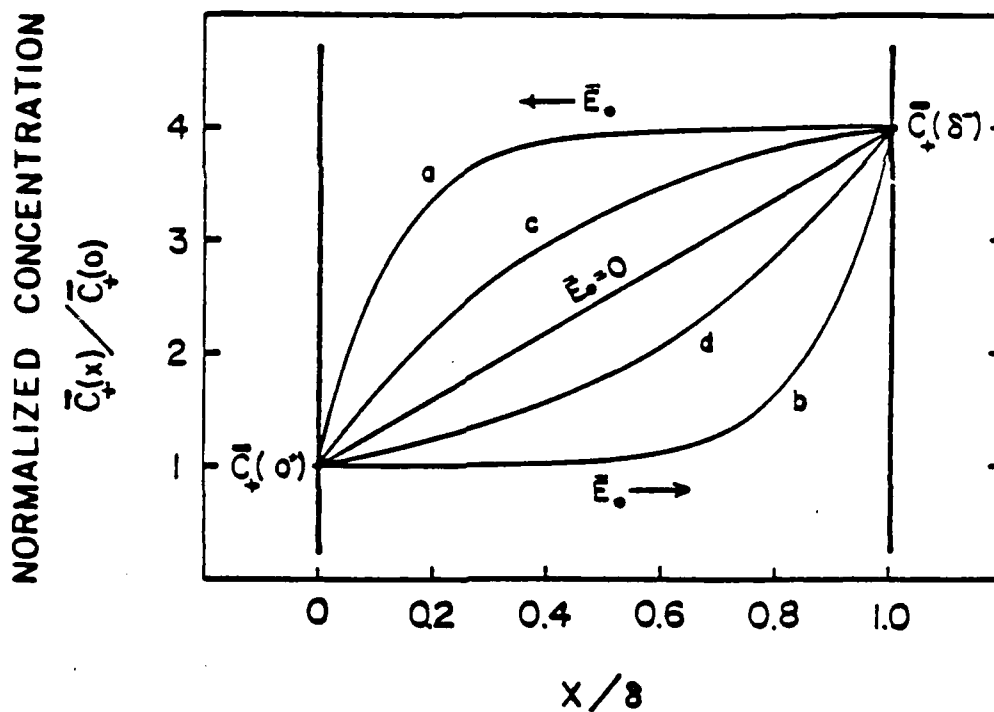


Figure 5. Basic electrodiffusion phenomenon. A positively charged membrane separates two salt baths of differing concentrations. The steady-state normalized co-ion concentration profile is plotted against normalized position within the membrane. At no applied field, the co-ion profile is approximately linear. As a stronger field is applied from left to right, the profile within the membrane is depleted. As a stronger field is applied from right to left, the profile within the membrane is enhanced.

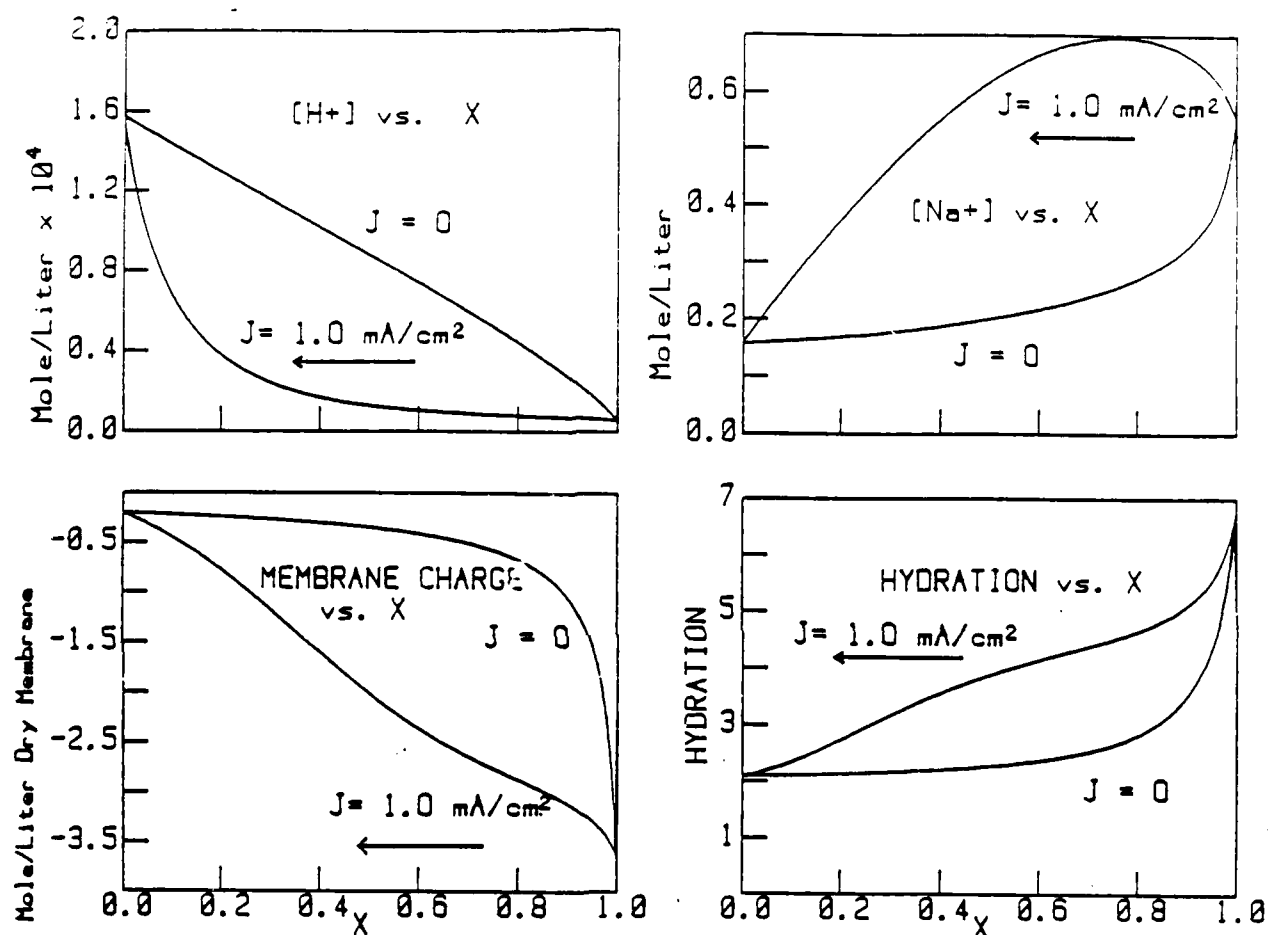


Figure 6. Basic electrodiffusion transduction phenomenon. A membrane with carboxylic acid sites separates two baths of differing pH. The left-hand bath is at pH 3.5 and the right-hand bath is at pH 6. The steady state concentrations of hydrogen ion, sodium (counter) ion, membrane fixed charge and hydration are plotted against normalized position within the membrane. At no applied field, the hydrogen ion profile is approximately linear. As a field is applied from right to left, the hydrogen ion concentration within the membrane is depleted, leading to increased fixed charge and increased membrane hydration.

Each component is modelled using simple linear laws. The effective diffusivity and mobility have porosity and tortuosity factors[8] in the implementation of the model. Continuity equations are written for each solute in the frame of the solid, the ψ frame. The standard time derivative is on the left, plus an additional bound solute term to account for the reaction of, e.g., hydrogen ions with carboxylic acid sites. Electroneutrality is assumed on the length scales of interest. Note that the fixed charge is written in units of $\frac{\text{molescharge}}{\text{litersolid}}$ and thus is divided by the hydration H to yield $\frac{\text{molescharge}}{\text{literfluid}}$. A membrane charging isotherm is written using a Langmuir isotherm, and this isotherm is also used for calculating the bound hydrogen ion. Finally Donnan partitioning is used to relate the interior concentrations just inside the membrane to the bath concentrations.

Figure 8 shows the general form of the electromechanical equations. Darcy's law is used to model fluid flow due to gradients in fluid pressure. Friedman showed that the use of this simple form of Darcy's law rather than a more detailed balance of momentum transfer is in general justified[6,7]. Fluid pressure can include hydrostatic pressure and also an "osmotic pressure" term, scaled by a reflection coefficient. The Darcy permeability coefficient, k , will in general be a function of local hydration.

Both the membrane solid component and the fluid are modelled as incompressible, so a volume continuity equation is straightforward. Since the local membrane hydration can change significantly, the equations are written in the frame of the solid, the ψ frame. A constitutive law relating the membrane swelling pressure p to the local ionic concentrations and local hydration is also needed. Here it is written in general form, and includes a purely mechanical term (f_1) and an electrostatic term (f_2). More details about the actual constitutive law used are described next. Finally, inertial terms are neglected and conservation of momentum is written for the membrane, letting us relate gradients in fluid pressure and the membrane swelling pressure.

Figure 9 gives more details on the electromechanical constitutive law used to model the membrane. The attractive force is calculated using a linear Hooke's law with a constant modulus. The electrostatic repulsion forces are estimated using a linearized flat plate double layer repulsion model. The net swelling pressure is the total of the purely mechanical pressure and the electrostatic repulsion pressure. The following equation gives the form of the electromechanical constitutive law actually used:

$$p = M' \left[H_0 - H_1 c_m'^2 \exp \left(H \frac{l_r}{l_D} \right) \right]$$

where M' is a normalized modulus, H_0, H_1, l_r are material constants, c_m' is the membrane charge density normalized to the solid content, and l_D is the local Debye length.

ELECTROMECHANICS OF CHARGED MEMBRANES

Electrochemical Equations

$r_i = -\bar{D}_i \frac{\partial \bar{c}_i}{\partial x} + \bar{u}_i \frac{z_i}{ z_i } \bar{c}_i E + \bar{c}_i U$	Solute Flux
$\frac{\partial}{\partial t} (H \bar{c}_i + H \bar{c}_i^b) = \frac{\partial r_i}{\partial x}$	Solute Continuity
$\sum z_i \bar{c}_i + \frac{z_m \bar{c}_m}{H} = 0$	Electroneutrality
$\bar{c}_m = -\bar{c}_m^s \frac{K}{K + \bar{c}_H}$	Membrane Charge Group Isotherm
$\bar{c}_+^{in} \bar{c}_-^{in} = \bar{c}_+^{out} \bar{c}_-^{out}$	Donnan Partition (Boundary Condition)

Figure 7. The general electrochemical equations for the membrane model. Solute flux includes terms for diffusive, migratory and convective flow. Solute continuity is written in the frame of the solid and includes a bound solute term. Electroneutrality over length scales of interest is written using fixed charge normalized to solid content. A Langmuir isotherm is used to model the dependence of membrane charge on local pH. Donnan partitioning relates the boundary conditions just inside the membrane with the external bath conditions.

ELECTROMECHANICS OF CHARGED MEMBRANES

Electromechanical Equations

$U = k \frac{\partial}{\partial x} (P - \Delta \pi)$	Darcy's Law (Fluid Flow)
$\frac{\partial H}{\partial t} = - \frac{\partial U}{\partial x}$	Fluid Mass Continuity
$p = f_1(H) - f_2(H, c_1) e^{-\alpha(H)}$	Membrane Swelling Constitutive Law
$\frac{\partial}{\partial x} (p + (P - \Delta \pi)) = 0$	Conservation of Momentum

Figure 8. The general electromechanical equations for the membrane model. They include a fluid flow constitutive law, an equation of fluid mass continuity written in the frame of the solid, a membrane swelling constitutive law and conservation of momentum, ignoring inertial terms and the transport of momentum by the fluid.

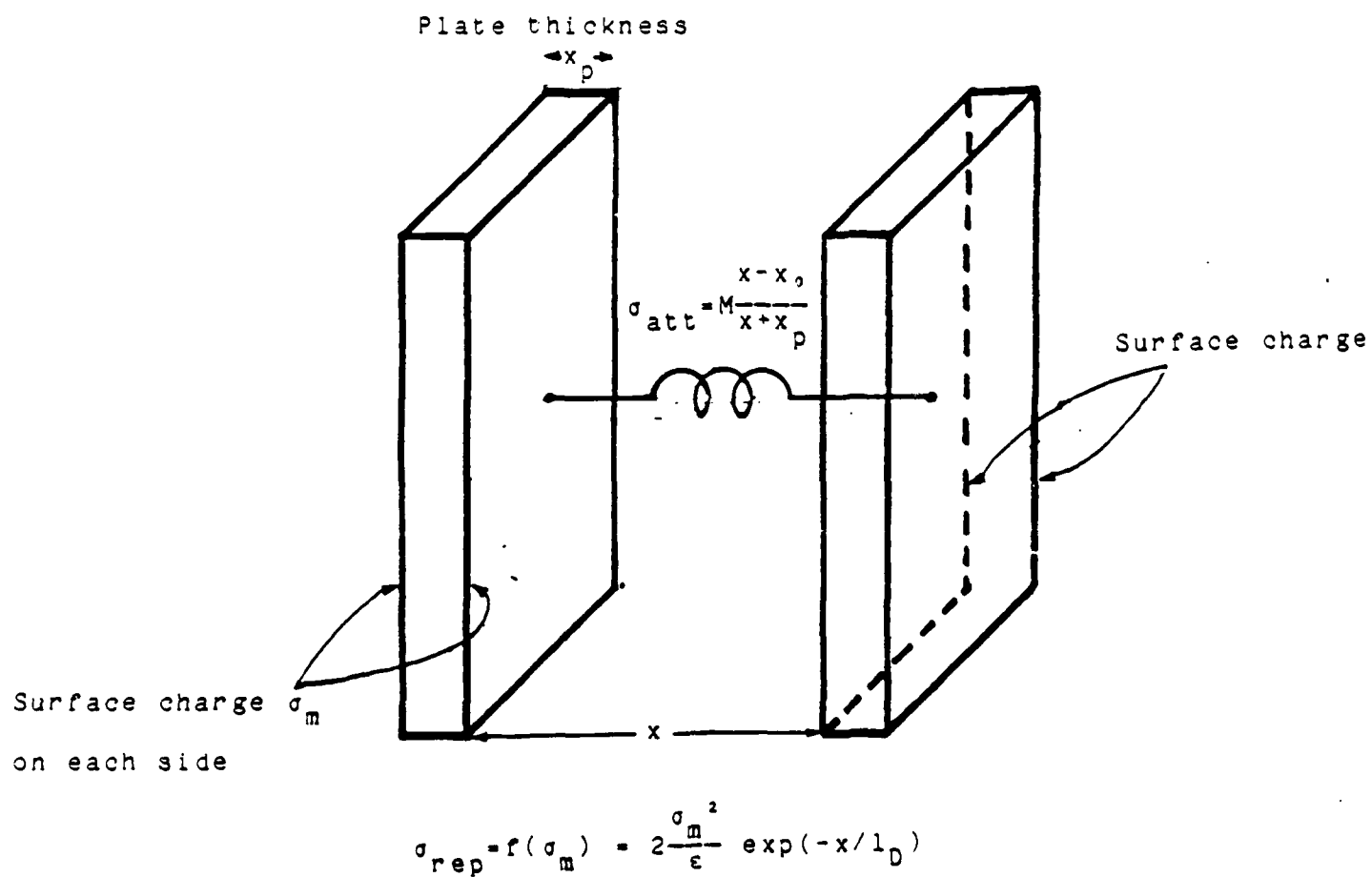


Figure 9. Some details of the micromodel used for the derivation of the electromechanical constitutive law used in the simulations.

CASE STUDY

It is instructive to examine a case study of the effects of an applied electric field on membrane properties. Figure 10 shows a membrane separating two baths at pH 6, with salt concentrations of 0.01 M on the left and 1.0 M on the right. The membrane parameters used in the model are listed in the center, and the calculated boundary conditions just inside the membrane are listed on either side of the membrane. This problem was solved numerically to determine the concentrations and hydrations profiles in steady state, both in the absence of an applied electric field and in the presence of an applied field.

Figure 11 shows some of the highlights of the steady state results. In the absence of an applied current, the hydrogen and chloride ion concentrations are fairly linear, except just at the boundaries. The hydration at the left boundary is high, because of the low salt concentration and consequent large Debye length. As the chloride ion concentration increases, the Debye length rapidly decreases, resulting in a large decrease in hydration moving into the membrane from the left boundary. As a field is applied from left to right, both the hydrogen and chloride ion concentrations within the membrane are enhanced. This response leads to decreased fixed charge and decreased Debye length. Thus, the charge effect and the Debye length effects combine to decrease the membrane hydration. When the field is reversed, the hydrogen and chloride ion concentrations within the membrane are depleted, leading to increased fixed charge and increased Debye length, and hence significantly increased hydration.

A more experimentally oriented view is given in Figure 12. Membrane thickness vs. normalized applied current is graphed, showing two saturation regions and a transition region around zero current. The scale is expanded on the right, showing the nonlinear response even around zero current. Similarly, the voltage vs. current relations show two saturation regions and a transition region. The expanded graph on the right shows the non-linear nature of the relationship even around zero.

We can also examine the dynamics of the membrane response using this model. Figure 13 shows the dynamic response of the average membrane hydration, chloride ion content, hydrogen ion content, and fixed charge density (normalized to membrane solid content) in time to changes in applied current. The membrane configuration is the same as in previous examples. At $t=1000$ hydrogen ion time constant factors, the current is turned on from right to left, reversed at 3×10^7 , and turned off at 6×10^7 . Time is normalized to the hydrogen ion diffusion time factor. There are two modes of response. The Debye length mode reaches steady state very quickly, as illustrated by the sharp edges in the chloride ion graph. The charge mode takes much longer, due to the long diffusion/reaction time, as seen from the rounded edges in the fixed charge vs. time graph.

The total membrane thickness can be measured experimentally; thus, the predictions of the model can be compared to experimental results. There was fairly

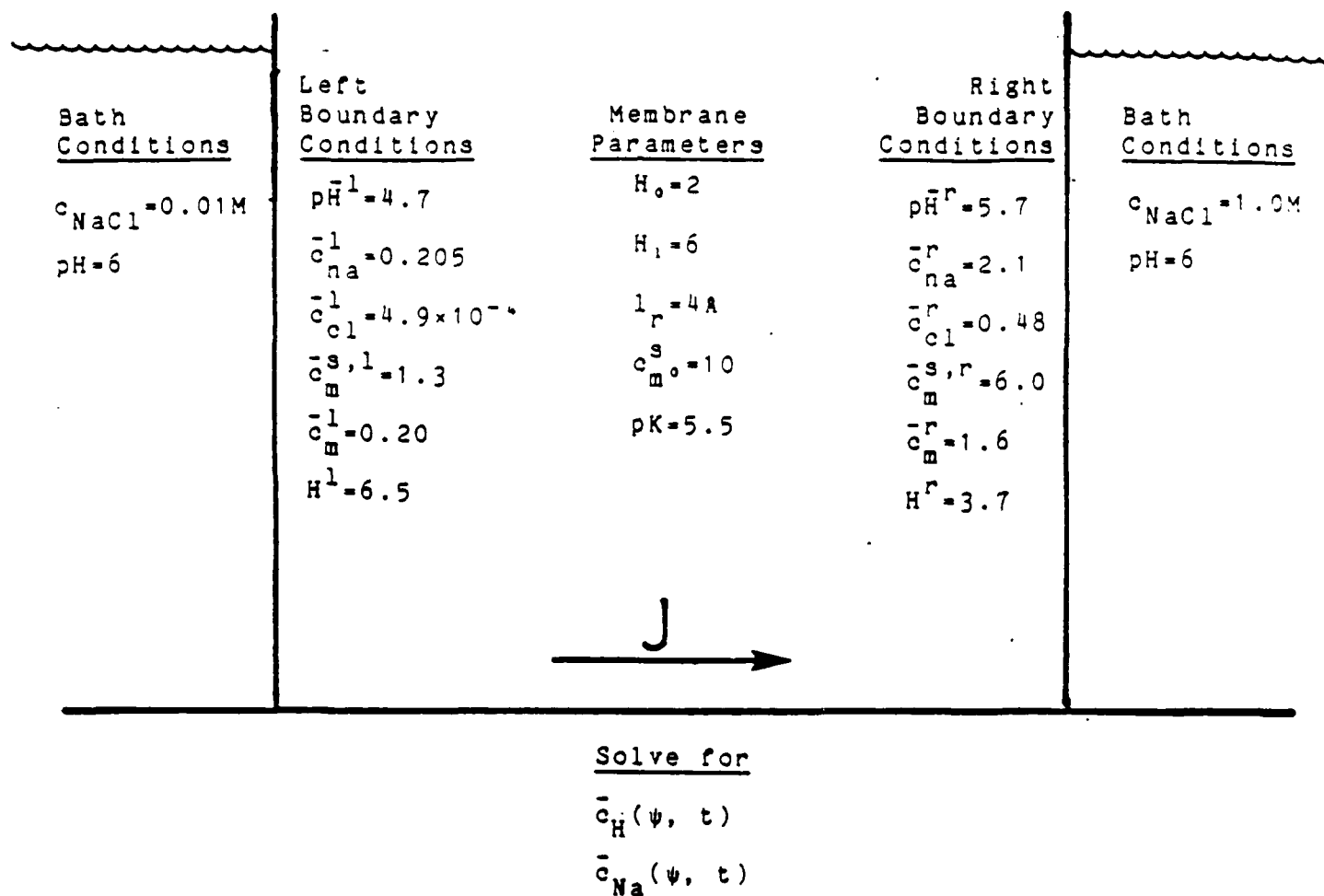


Figure 10. Case study of a membrane separating two baths of differing salt concentration. On the left the salt concentration is 0.01M, and on the right the salt concentration is 1.0M. The bath pH is 6 on either side. The membrane has a charge site density of 10 moles per liter dry membrane, and the average pK is 5.5. The electromechanical constitutive law parameters are $H_0=2$, $H_1=6$ and $l_r=4$ angstroms. This corresponds roughly to certain synthetic polyelectrolyte hydrogel membranes. The calculated boundary conditions just inside the membrane are calculated using Donnan equilibrium relations, electroneutrality, and the electromechanical constitutive law.

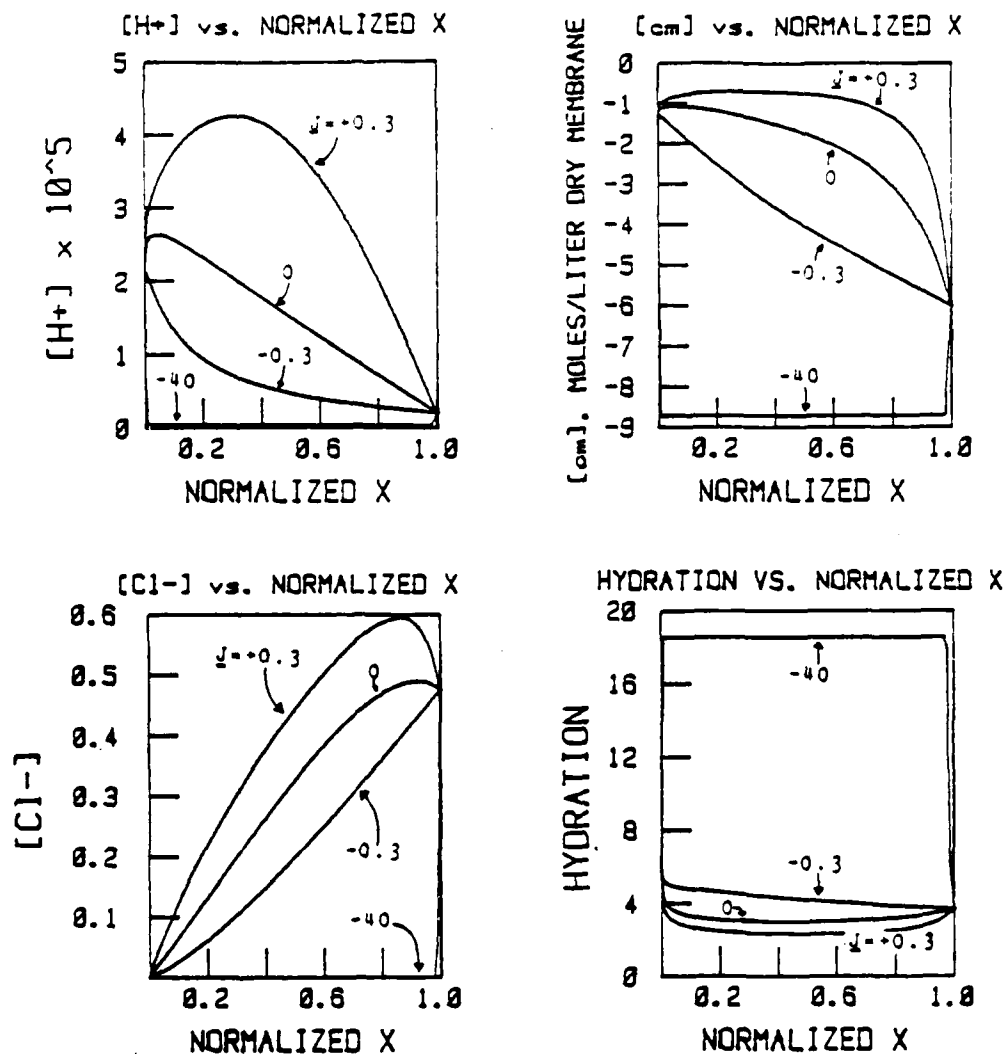


Figure 11. Steady state concentrations and hydration profiles vs. normalized position within the membrane for the case illustrated in the previous figure.

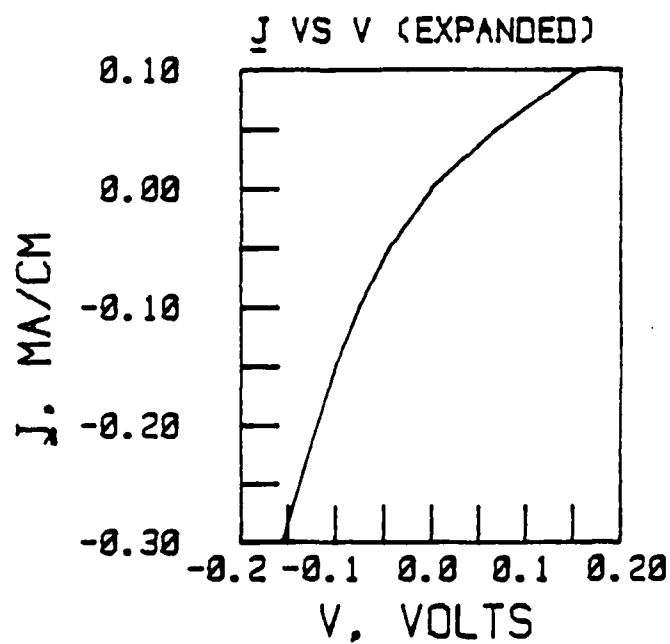
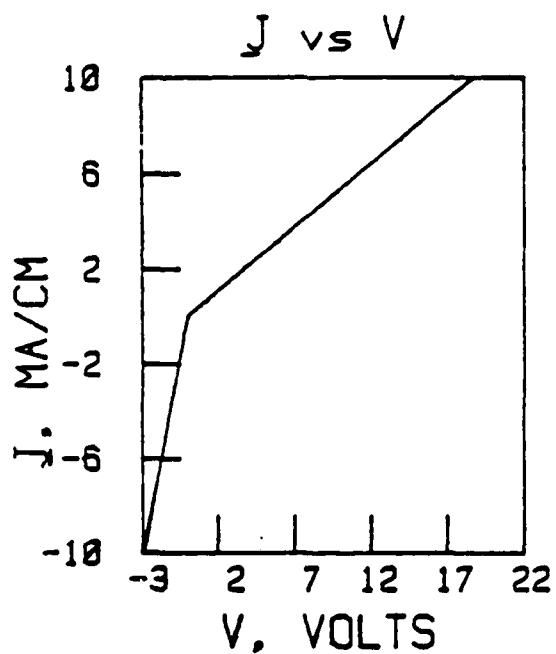
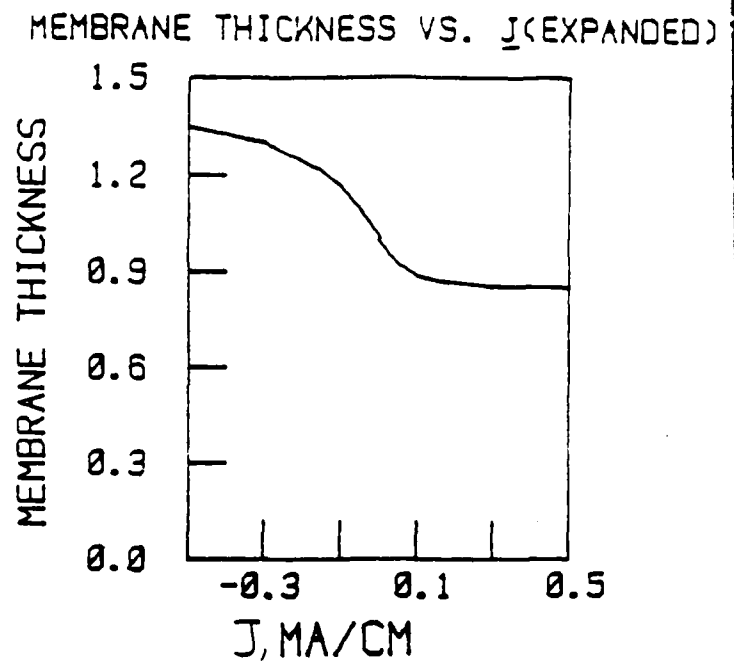
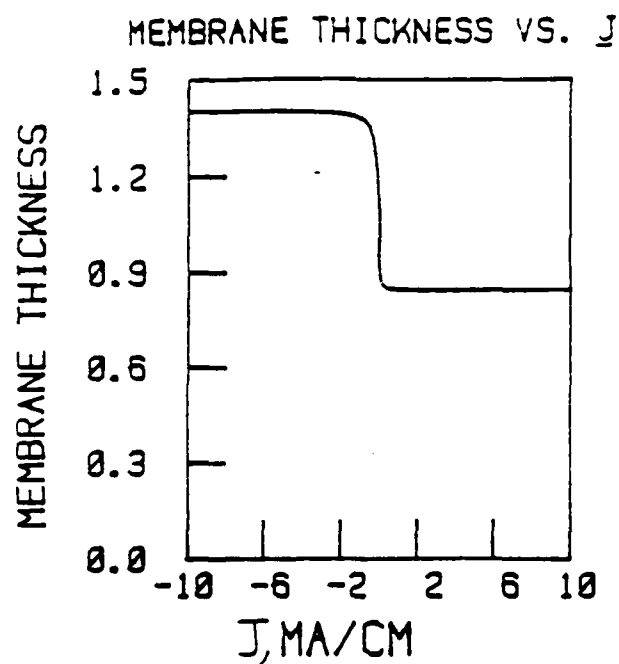


Figure 12. Steady state total membrane thickness vs. applied current, and steady state current vs. voltage relationships for the case previously illustrated.

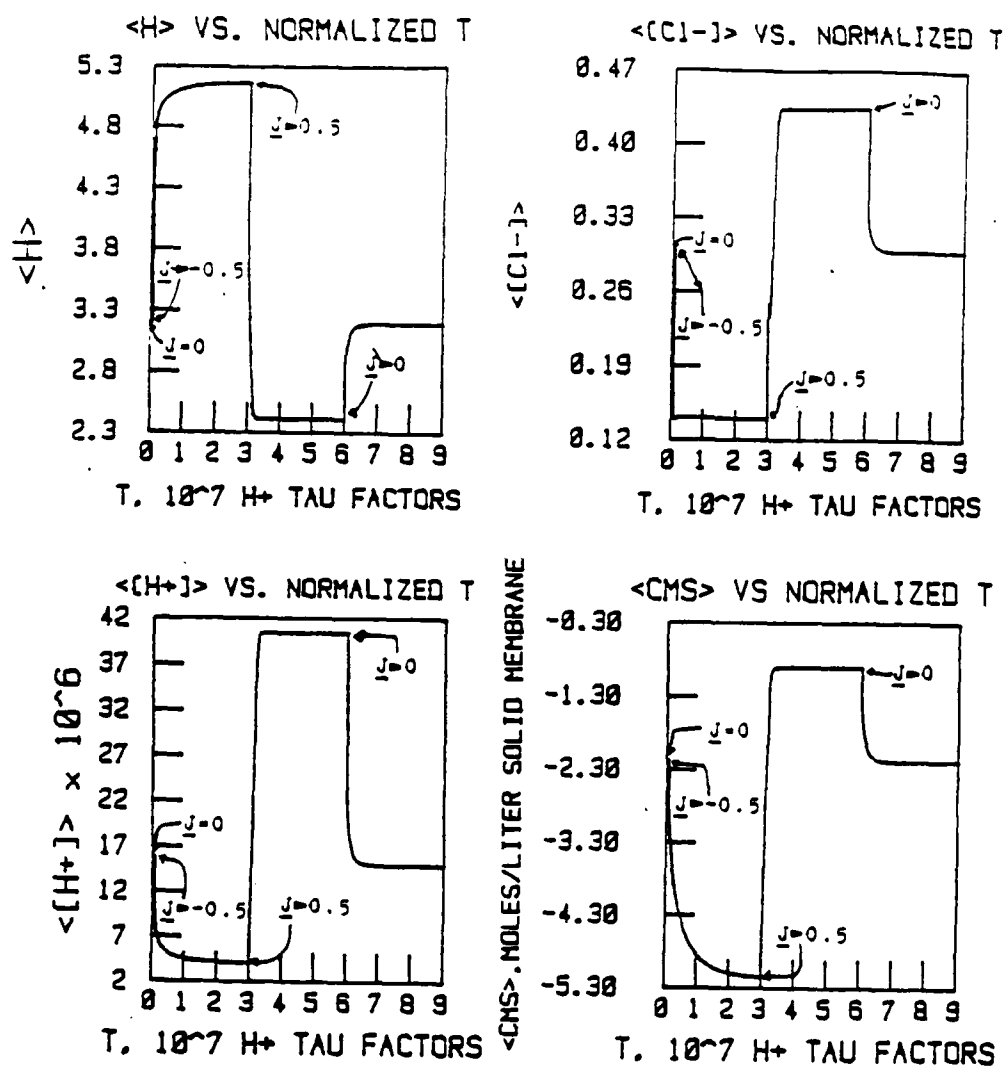


Figure 13. Dynamic response of average hydration, chloride and hydrogen ion concentration and fixed charge concentration to changes in applied current.

good correlation of theory and experiment, as shown in Figure 14 from reference 3. The direction of change and the extent of rectification phenomenon are predicted well by the theory. In these dynamic simulations, only the electrochemical dynamics (and not the mechanical dynamics) are included; the approximation of mechanical quasi-equilibrium was made. It is quite clear from these graphs that the mechanical dynamics are important in accurately modelling the membrane response under the experimental conditions. They constitute another rate-limiting process which can affect the transient response to step inputs (frequency response to sinusoidal inputs).

APPLICATION OF THEORY TO BIOLOGICAL CASES

The basic general theory described in the previous section can be applied with some modifications to certain aspects of biological response to applied electric fields. We will examine some of the possible sites of the effects of electric fields on living tissues and the possible transduction mechanisms.

Figure 15 [2] shows a schematic of a cell membrane. The resistance of the phospholipid bilayer region to ionic flow is very high, so we expect almost all of the ionic transport across the cell membrane to occur in special protein channels which are additional structures incorporated in the basic bilayer structure of the cell membrane. In this picture, a cell channel consisting of a tetrameric ionophore is illustrated, which can let ions pass through in the interior hydrophilic region of the protein. Changes in the ionic flow rates and/or changes in the ionic composition of the cell cytoplasm could result in changes of metabolic/enzymatic rates, or even which products are produced. Other feedback and coupling could amplify these effects.

Figure 16 shows a number of different models of cell membrane ion channels. In all of these models, the cell channel might be viewed as part of a membrane whose porosity, tortuosity, fixed charge density, and reflection coefficient is space varying. One could apply the model that has been developed to the problem of a sinusoidal field applied across a cell membrane. The details of the electromechanical coupling would have to be tailored to the actual cell channel type, as more information becomes available. A possible mode of coupling could be a conformational change of the cell channel protein, which depends on the ionic environment near one or more charge sites. Perhaps the percentage of open channels will be related to the average ionic concentration at some distance within the cell channel, which could be modulated by an applied electric field through electrodiffusion.

In general, electric fields modulation of cell channel permeability and configuration can affect any cell, including nerve cells. Nerve cell interconnections, shown in Figure 17, can also be affected by an applied electric field through electrodiffusion effects. Nerve impulse generation rates and their sensitivity to other environmental factors could be affected by electrodiffusion induced permeability changes. In addition, the actual propagation rate and distance may be affected by changes in the

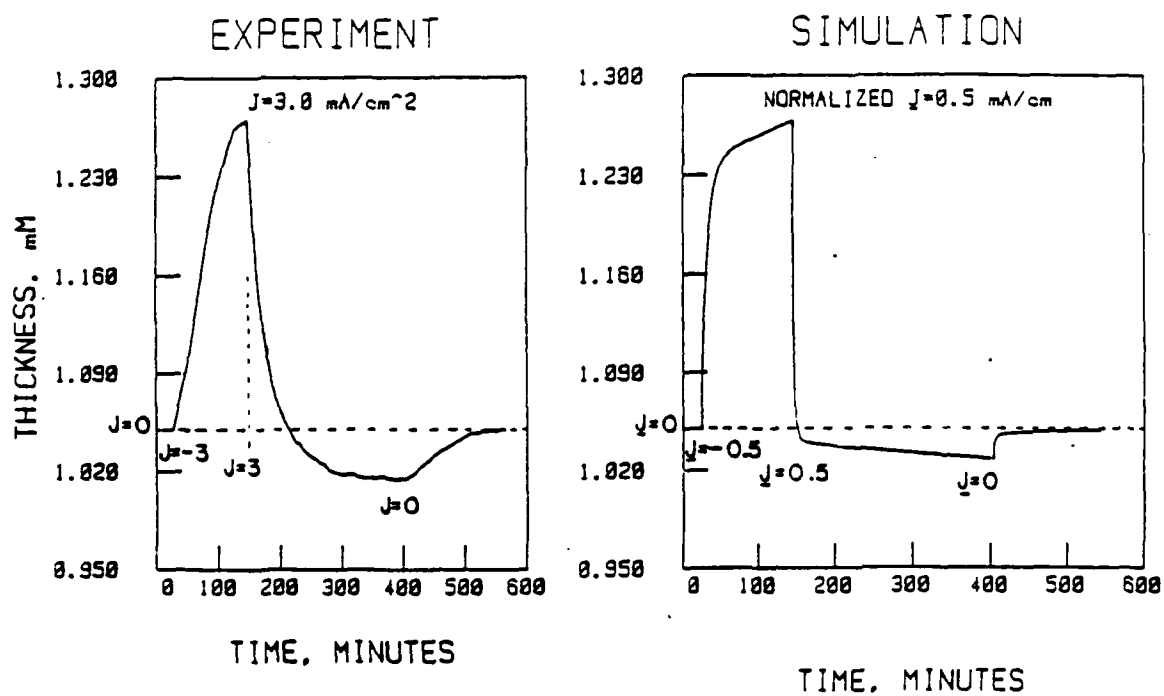
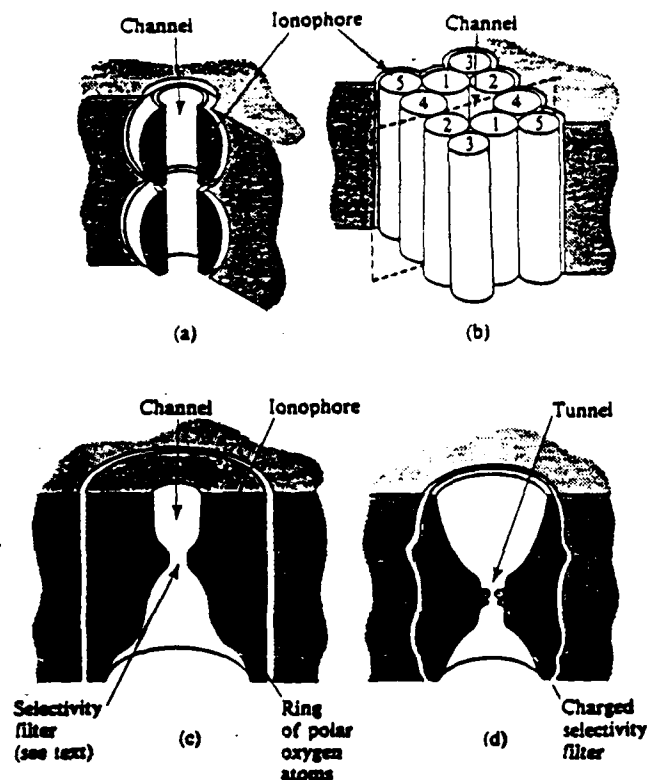


Figure 14. Comparison of experimental results of membrane swelling vs. time in response to step jumps in applied current to simulation results. The simulations used the approximation of mechanical quasi-equilibrium.



Ion channel models. **a** Tubular ionophore. Shown is the channel formed by the antibiotic gramicidin, two molecules of which are needed to span the membrane. **b** Rodlike ionophores. Shown is a proposed organization of the anion channel in the red blood cell (Solomon et al. 1983). The ionophore is a dimer. Each monomer consists of five rodlike helices. Three helices (1, 2, and 4) from each monomer surround the pore. **c** Potassium-selective channel in nerve (Latorre and Miller 1983). The selectivity filter does not pass Li or Na readily because they do not fit through in their hydrated forms. Unhydrated, Li and Na are too small to interact fully with the ring of oxygens at the throat of the filter. Transport through this channel is thought to proceed by single-file diffusion, with perhaps three potassium ions in the channel at any time. **d** Sarcoplasmic reticulum maxi-potassium channel, redrawn from Miller (1982). The tunnel is occupied by no more than one ion at a time. As in **c**, diffusion is relatively unrestricted at the mouths of the pore. The channel in this cartoon is drawn to scale.

Figure 16. Different views of cell channel structures, taken from [2].

permeability of the axolemma and changes in the ionic composition of the axoplasm and the extracellular fluid. In myelinated neurons, the effects would be concentrated in the nodes of Ranvier.

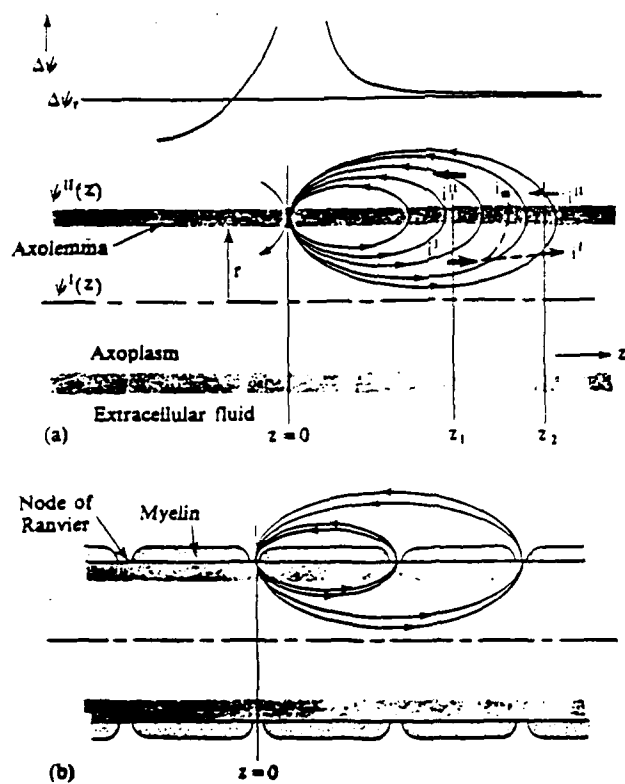
Epithelial membrane is another possible site of electric field modulation of membrane permeability. Epithelial membranes, an example of which is shown in Figure 18, consist of many interconnected cells on top of a basement membrane. A simplified schematic of epithelial membranes is shown in Figure 19. The path through epithelial membranes consists of transcellular paths in parallel and in series with intracellular paths. Electric field mediated electrodiffusion could affect the permeability of the cell membranes, as previously discussed, as well as the permeability of the apical membrane, the junctions, and the paracellular space.

Figure 20 shows a sample pathway for sodium ions through tight epithelia. Sodium is actively transported into the cell through the apical membrane, and actively transported out through the active sodium-potassium pump. Sodium also diffuses passively through the basolateral membrane. Electric field modulation of any of the transport rates could affect net transport rates. Over time ionic concentrations on either side of the membrane could deviate significantly from their normal concentrations, possibly leading to significant changes in other transport rates and/or metabolic rates and products.

SUMMARY

We have shown that electric fields can modulate intramembrane ionic concentrations, transmembrane ionic fluxes, the mechanical conformation of the membrane, and the transmembrane potential. Even symmetrically applied fields of opposite polarities can result in asymmetric mechanical, concentration and flux responses, hence rectification of electrochemical and electromechanical phenomena can produce long-term effects even though the induced change is small. We have developed a general electromechanochemical model which predicts rectification phenomena that includes the mechanical and electromechanical conformational change dynamics.

To put in perspective the frequency response associated with the electrodiffusion mechanism, we first focus on the electrodiffusion curves of Figure 5. In the absence of an applied field, the concentration profile shown in the figure is linear. A step field in the x direction having a small magnitude of approximately $25 \text{ mV}/(\text{membrane thickness } \delta)$ will shift the concentration profile to curve d. For small enough applied field, the time dependence of this linearized shift is described by a series solution characterized by the leading exponential relaxation time τ_{ed} approximately equal to $\delta^2/(\pi^2 D)$. (This is essentially the diffusion time for a solute of diffusivity D .) Larger applied fields will produce a nonlinear response whose time dependence is more complicated, but can be computed via our model. A description of frequency response can be made most easily in terms of the linearized model, since the frequency is related to the inverse of the electrodiffusion time constant.



Propagation of the action potential along: a an unmyelinated neuron; b a myelinated neuron. The action potential is at $z = 0$ and is propagating to the right. Dashed lines in a illustrate Eq. (7.23).

Figure 17. Schematic of nerve impulse propagation[2].

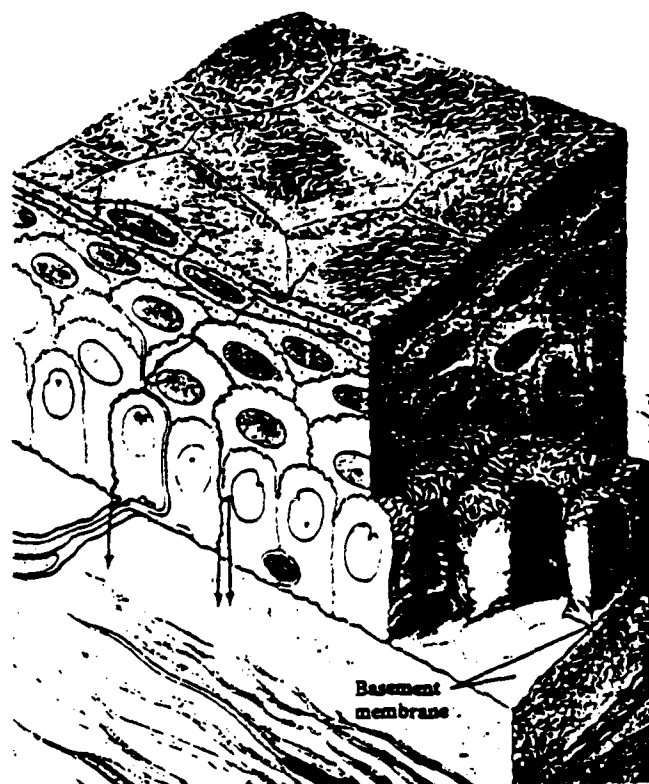
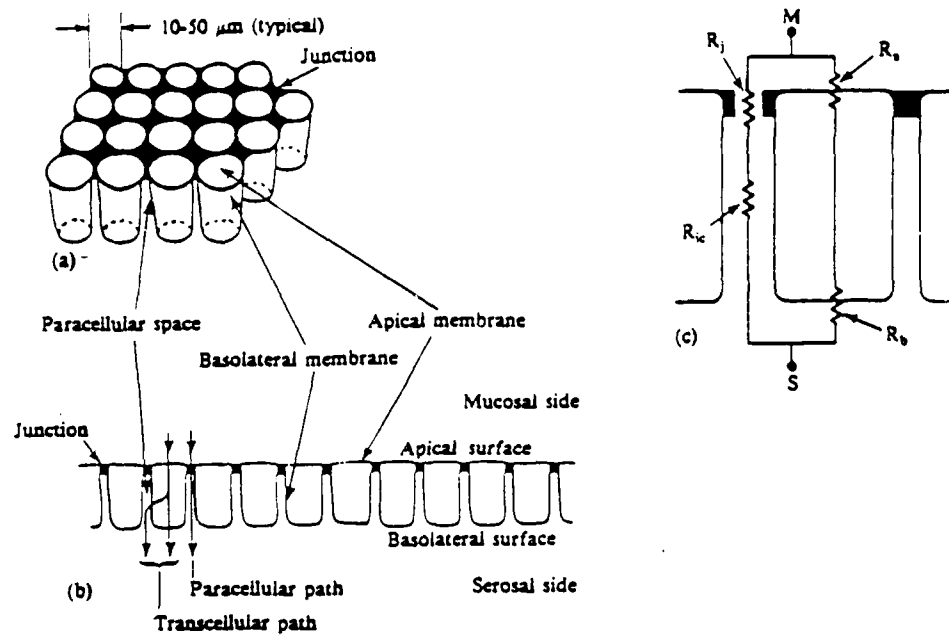
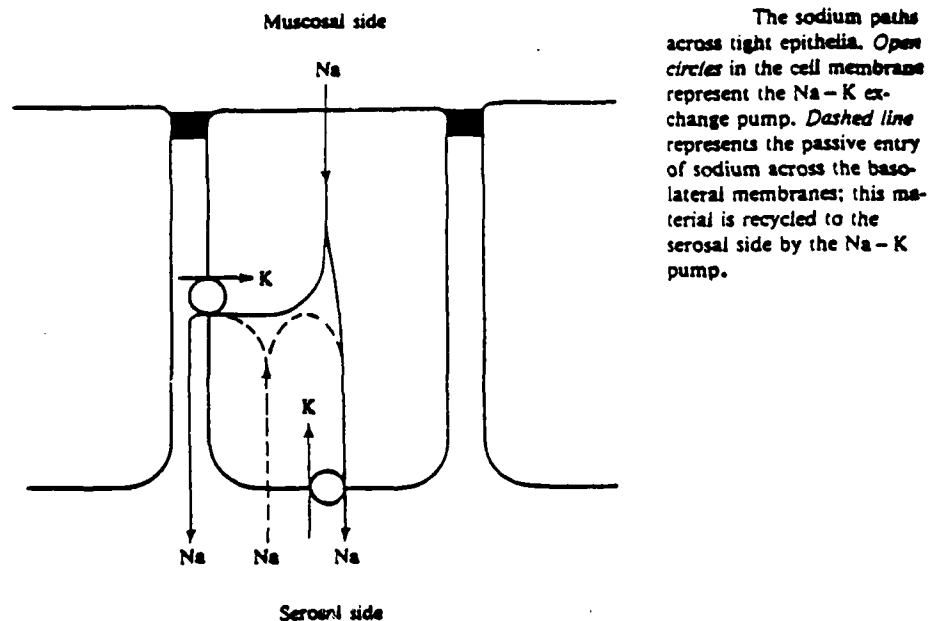


Figure 18. Illustration of epithelial membrane[2].



A monolayer epithelium. a View from the mucosal side. b Section through the cells. Here and in the figures to follow, the space between the cells is enlarged for clarity. The cells are much more closely packed in real epithelia, their surfaces are more irregular, and the path between them is more tortuous. The cells are supported at their basal surfaces by a basement membrane, not shown. c The equivalent resistances of the pathways across the epithelium. R_e is the resistance of the intercellular channel; the meaning of the other subscripts is obvious.

Figure 19. Schematic of epithelial membrane and the available transport paths[2].



The sodium paths across tight epithelia. Open circles in the cell membrane represent the Na-K exchange pump. Dashed line represents the passive entry of sodium across the basolateral membranes; this material is recycled to the serosal side by the Na-K pump.

Figure 20. Schematic of sodium transport paths through tight epithelia[2].

Given the form of τ_{ed} , electrodiffusion-induced changes in intramembrane concentrations will be slower with increasing thickness and with decreasing diffusivity. Thus, thinner membranes will exhibit electrodiffusion phenomena at higher frequencies by the square of the thickness. In Figure 14, for example, the simulation was computed on the basis of a 1 mm thick "membrane" (i.e., a very thick section of extracellular matrix). Electrodiffusion-induced changes at the 15 per cent level took approximately 5 min, corresponding to an upper cutoff frequency of a few mHz. However, when the same simulation is scaled to a thickness of 1 μm or 10 nm (cell membrane thickness), the cutoff frequency would be 1 kHz and 10 MHz, respectively. Similarly, for thicknesses on the order of a cell membrane, each horizontal time division in Figure 13 would scale to 1 ms while a 1 μm thickness would correspond to 10 s per division.

Thus, when electrodiffusion is considered under linearized operation, frequencies up to 10-100 MHz may be of interest. As discussed in previous progress reports, however, nonlinear operation is very common and to be expected for asymmetric systems such as that of Figure 10 (the case of a salt concentration gradient across the membrane). Under such conditions, the very small changes that would be produced at even higher frequencies might accumulate due to membrane rectification.

ACKNOWLEDGMENTS

We would like to acknowledge the technical assistance of E. Paul Warren and the excellent editorial and administrative assistance of Linda D. Bragman.

REFERENCES

1. Hille, B., *Ionic Channels of Excitable Membranes*. Maine: Sinauer Associates, 1984.
2. Friedman, M.H., *Principles and Models of Biological Transport*. Berlin: Springer-Verlag, 1986.
3. J.H. Nussbaum. *Electric Field Control of Mechanical and Electrochemical Properties of Polyelectrolyte Gel Membranes*, Sc. D. thesis, Massachusetts Institute of Technology, Cambridge, 1986.
4. Oosawa, F., *Polyelectrolytes*. New York: Marcel Dekker, 1971.
5. Tanford, C., *Physical Chemistry of Macromolecules*. New York: Wiley, 1961.
6. Friedman, M. H. Free Swelling of Biological Tissue: The Corneal Stroma, *Chem. Eng. Prog. Symp. Ser.*, 66: 33-42 (1970).

7. Friedman, M. H. General Theory of Tissue Swelling With Application to the Corneal Stroma, *J. Theor. Biol.* 30: 93-109 (1971).
8. Mackie, J. S. and Meares, P. The Diffusion of Electrolytes in a Cation-Exchange Resin Membrane, *Proc. Royal Soc. A* 232: 498-509 (1955).